INTERNATIONAL JOURNAL OF FLUID POWER, 2017
VOL. 18, NO. 2, 92–101
https://doi.org/10.1080/14399776.2016.1265875

Taylor & Francis
Taylor & Francis Group

Check for updates

Introduction, mathematical modelling and motion control of the novel pneumatic textile actuator

Michael Heidingsfeld[a], Ryosuke Horio[b], Bastian Baesch[c], Christoph Riethmüller[c], Götz T. Gresser[c] and Oliver Sawodny[a]

[a]Institute for System Dynamics, University of Stuttgart, Stuttgart, Germany; [b]Systems Engineering Laboratory, Department of Mechanical Engineering, Toyohashi University of Technology, Toyohashi, Japan; [c]Institute of Textile Technology and Process Engineering Denkendorf, Denkendorf, Germany

ABSTRACT

This paper introduces a novel type of pneumatic actuator, namely the pneumatic textile actuator (PTA). Although the operating principle is similar to pneumatic artificial muscles, design, fabrication and properties of PTAs show significant differences. PTAs consist of double-layered textiles, fabricated in one piece using the Jacquard weaving technology. By filling the chamber between the two layers with pressurised air, one obtains a low-weight, high-power pneumatic actuator at very low cost. The paper first describes the design, fabrication and properties of PTAs in general. Then, the characteristics of a specific PTA are determined experimentally. Moreover, we derive a mathematical model of the dynamic behaviour of the PTA. The model forms the basis for a motion control algorithm, combining flatness-based feedforward and linear feedback control. Finally, the performance of the controller is evaluated experimentally. The results indicate that PTAs are well suited for motion control tasks requiring small displacements but high forces and minimum actuator weight.

ARTICLE HISTORY
Received 2 August 2016
Accepted 22 November 2016

KEYWORDS
Pneumatic actuators; artificial muscles; motion control; differential flatness

1. Introduction

Pneumatic actuators are commonly used when high-power densities and a clean working medium are required. There are many types of pneumatic actuators, such as conventional pneumatic cylinders or pneumatic vane motors. Pneumatic artificial muscles (PAM), also known as McKibben muscles, are a special type of actuators where an elastic tube is filled with pressurised air. The contraction of the tube translates to a linear motion of the actuator. Besides the McKibben design, there exist a number of different PAMs with their respective strengths and weaknesses (see e.g. Daerden and Lefeber (2001) for a more detailed discussion). The present paper introduces a novel type of pneumatic actuator, namely the pneumatic textile actuator (PTA), developed by the Institute of Textile Technology and Process Engineering Denkendorf. The operating principle of PTAs is similar to PAMs. However, their design, fabrication and properties show significant differences. Jacquard weaving technology allows the production of fabrics with enclosed chambers that can be made airproof and filled with fluids. When such a chamber is filled with compressed air, it expands perpendicularly to the fabric plane. This leads, due to the bulging of the fabric's surfaces, to an in-plane contraction (Figure 1). With the proper layout of the chamber(s), compressed air connections and force transmission elements, this effect can be used to create a low-weight, high-power pneumatic actuator at very low cost. In the first part of the paper, the operating principle, properties and fabrication process of PTAs are introduced (Section 2). Moreover, the characteristics of a specific PTA are determined experimentally (Section 3). The second part of the paper aims at the design of a model-based motion controller to demonstrate the performance of PTAs. To do so, a mathematical model of the dynamic behaviour of PTAs is derived (Section 4). Based on the model, we design a motion controller, combining flatness-based feedforward and linear feedback control (Section 5). Finally, the performance of the PTA in combination with the suggested controller is evaluated experimentally (Section 6).

2. Pneumatic textile actuators

PTAs are made by Jacquard weaving. This technology enables the creation of flat fabrics, whose yarns can form one or several interconnected layers at every crosslink between warp and weft. Due to the high demands on single yarn tension control in the process of weaving, the different layers can be designed with very uniform stress–strain characteristics. Due to the crosslinking of the yarns between different fabric layers at the layers'

CONTACT Michael Heidingsfeld heidingsfeld@isys.uni-stuttgart.de

© 2016 Informa UK Limited, trading as Taylor & Francis Group

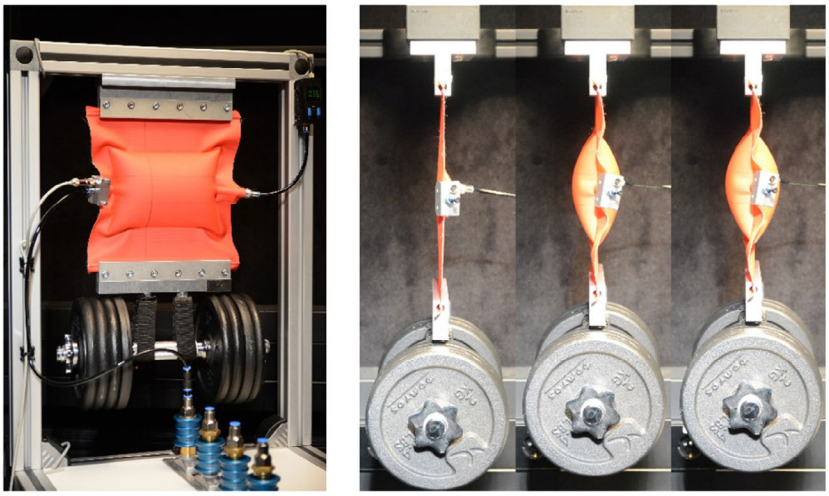

Figure 1. Novel pneumatic textile actuator (PTA) developed by the Institute of Textile Technology and Process Engineering Denkendorf, Germany.

interconnections, such connections can bear much higher forces as could be achieved with other processes like adhesive bonding or sewing. Electronically controlled healds in modern Jacquard looms enable the production of CAD-designed multi-layered fabrics with arbitrarily shaped chambers. To produce PTAs, the fabric is made air proof by film lamination on both fabric sides in an additional process. Single actuators can be cut out of the laminated fabric using an automated laser cutting machine. A PTA is completed by adding compressed air connections and force transmission elements. The force transmission elements can consist of woven gutters, laminated layers of fibre composite materials or other connection elements like clamping devices. By producing the PTAs fabric out of high modulus polyester fibres, the production process can be very economic. Compared to the prices in similar textile processes like one-piece woven airbag production, PTAs can be produced in a very low price range. Using standard weaving technology, it should be possible to easily create PTAs with air chamber sizes of about two metres width and decades of metres in length. With special machines one cold even imagine PTAs with much bigger dimensions.

Compared to conventional pneumatic actuators, i.e. pneumatic cylinders, PTAs have quite different kinematics and mechanical characteristics. PTAs consist of fabric and therefore can transmit pulling forces only. The maximum contraction of a PTA lies at about 33%. This is caused by geometry. Ideally, the bulging chamber layers form a circle when inflated. This means the deflated rectangular PTAs initial length is half the circumference of the resulting cross section. The minimum PTAs length is the resulting circles diameter. In reality, the form of the inflated PTA deviates from the ideal circle, which leads to a reduction in the maximum contraction.

In a conventional pneumatic cylinder, the piston surface determines the actuators maximum force and is only a small part of the actuators whole inner surface. In PTAs, the whole surface of the pressure chamber is working as force transmitting element. This leads to high forces even at low inner pressures. A PTA with a 200 × 200 mm sized air chamber can transmit forces up to 3500 N at about 0.7 bar relative pressure. Due to the mechanism, the working surface changes its orientation with travel, which leads to a decreasing force of the PTA at increasing travel distance. Because there is no piston in a PTA, the energy dissipation is very low compared to conventional pneumatic cylinders. Friction occurs only between yarns at the interconnection of the double-layered chamber surfaces and in a very small-scale movement compared to the actuators travel. A main benefit of PTAs is not only the high force at low pressures, but the ultra-lightweight construction. A 200 × 200 mm PTA's maximum travel range is about 70 mm. Its total weight, including the connection parts, is about 65 g. A comparable conventional pneumatic cylinder weighs about 1800 g. This leads to a force/weight ratio of about 53 N/g of a PTA, compared to about 2 N/g of a pneumatic cylinder. Compared to McKibben PAMs, PTAs achieve higher contraction, resulting in more available actuator travel for actuators of the same length. Finally, PTAs can be designed with almost arbitrary two-dimensional initial geometries, including multiple pressure chambers and air supply lines.

3. Force and volume characteristics

In contrast to conventional pneumatic actuators, the tensile force F exerted by PTAs depends not only on the pressure p inside the pressure chamber but also on its contraction. Considering only one dimension of motion, we define the actuator travel $z = l_0 - l$ as the difference between the current length l and the initial length l_0 of the flat and unloaded PTA. Besides the force, also the volume V of the PTA's pressure chamber depends on pressure and actuator travel. The force and volume

Table 1. Mathematical symbols and their physical units.

Symbol	Unit	Description
t	s	Time
z	m	Actuator travel
l	m	Length of the PTA
l_0	m	Initial length of the PTA
V	m^3	Volume of the pressure chamber
F	N	Tensile force
p	Pa	Absolute pressure inside the pressure chamber
p_a	Pa	Absolute ambient pressure
p_s	Pa	Absolute supply pressure
p_{rel}	Pa	Pressure inside the pressure chamber relative to ambient pressure
m_l	kg	Load mass
d_l	N s/m	Viscous damping coefficient
k_l	N/m	Spring stiffness
T	K	Ambient temperature
m	kg	Gas mass inside the pressure chamber
R_s	J/mol K	Specific gas constant
g	m/s^2	Constant of gravity
χ		Isentropic exponent
ρ_a	kg/m^3	Density of dry air at ambient conditions
$\psi(p_1, p_2)$		Flow function
p_1	Pa	Primary/upstream pressure
p_2	Pa	Secondary/downstream pressure
b		Critical pressure ratio
$C(v)$	m^3/Pa s	Flow conductance
v		Normalised valve position
$\boldsymbol{x}, \boldsymbol{x}_d$		System state/desired value
$\boldsymbol{f}(\boldsymbol{x})$		Drift vector field
$\boldsymbol{g}(\boldsymbol{x})$		Input vector field
y, y_d		Controlled variable/desired value
u		Control input
u_{ff}, u_{fb}		Feedforward/feedback control portion
u_{max}, u_{min}		Upper/lower limit of the control input
k_P, k_I		Proportional/integral controller gain
$\boldsymbol{x}^*$		Flat coordinates
$\Phi(\boldsymbol{x}), \Phi^{-1}(\boldsymbol{x}^*)$		Transformation to flat coordinates/inverse transformation
$\alpha(\boldsymbol{x}), \beta(\boldsymbol{x})$		Short forms for the Lie derivatives of the flat output
T_1, T_2, T_3, T_4	s	Transition times

characteristics are governed by the elasticity of the fabric, as well as the change of the pressure chamber's geometry. Due to the very low mass of the fabric, inertial effects can be neglected, such that there exist static non-linear maps F(z, p) and $V(z, p)$.

Theoretical derivation of the non-linear force and volume maps for arbitrary two-dimensional initial geometries of the pressure chamber is a challenging task. Even for simple rectangular geometries, this employs the use of approximation methods like the finite element method. Therefore, the force and volume map of an exemplary 200 × 200 mm PTA were derived experimentally. The experimental data were obtained by measuring the force and volume for different combinations of actuator travel and relative pressure. For mathematical modelling and controller design, analytical expressions for $F(z, p)$ and $V(z, p)$ with certain demands on differentiability will be useful. Therefore, the data are fitted using multivariate polynomials of the form

$$F(z,p) = \sum_{i=0}^{n_{F,z}} \sum_{j=0}^{n_{F,p}} c_{F,ij} z^i \left(p - p_a\right)^j \tag{1a}$$

$$V(z,p) = \sum_{i=0}^{n_{V,z}} \sum_{j=0}^{n_{V,p}} c_{V,ij} z^i \left(p - p_a\right)^j \tag{1b}$$

where $n_{F,z} = 4$, $n_{F,p} = 2$, $n_{V,z} = 2$ and $n_{V,p} = 1$ are the degrees in z and p, respectively, and p_a is the ambient pressure. The coefficients $c_{F,ij}$ and $c_{V,ij}$ are obtained by least square regression. The resulting polynomials approximate the static force and volume map, as long as z and p stay within the data range (Figure 2). However, extrapolation beyond the given data should be avoided, since the fit may become inaccurate and even lose its physical meaning, e.g. the force may become negative, which is impossible due to the fact, that the PTA can only transmit tensile forces.

4. Dynamic model

The system under consideration consists of a 200 × 200 mm PTA in series with a mass–spring–damper element clamped to a rigid frame (Figure 3). A proportional control valve regulates the airflow to the pressure chamber. The pressure inside the chamber and the position of the mass are measured using a pressure and position sensor, respectively.

The dynamic model of the system consists of three parts, namely the equations of motion of the mass in terms of the position $z(t)$ (Section 4.1), the dynamics of the pressure

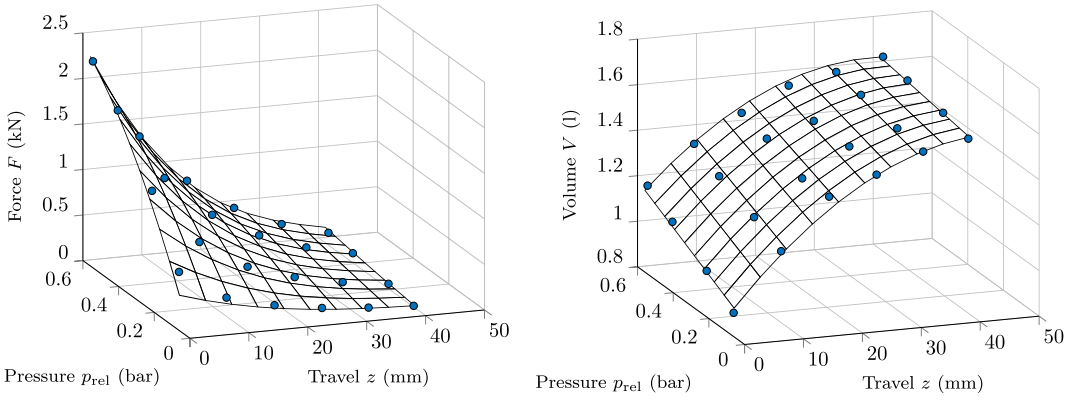

Figure 2. Experimental data (dots) and polynomial fits (mesh) of the non-linear force (left) and volume (right) maps of a 200 × 200 mm PTA, depending on the actuator travel z and relative pressure $p_{rel} = p - p_a$.

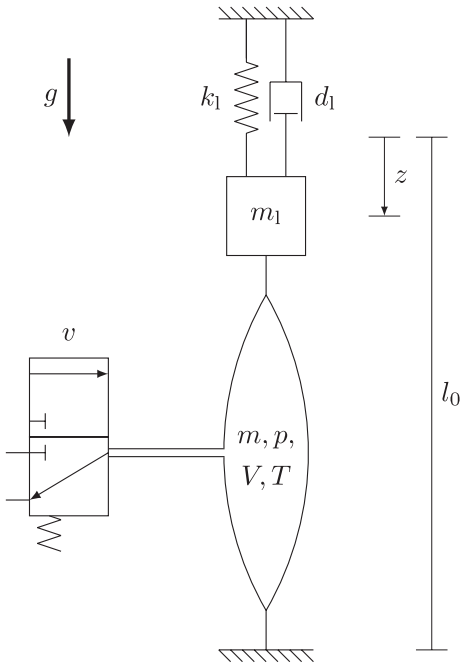

Figure 3. Schematic of the system.

$p(t)$ inside the PTA's pressure chamber (Section 4.2), and the valve model (Section 4.3). The mechanical and pneumatic parts are coupled via the tensile force $F(z(t), p(t))$ and the volume $V(z(t), p(t))$. In the following, whenever there is no ambiguity, the argument t is omitted for the sake of brevity. The mathematical symbols used throughout this paper are summarised in Table 1.

4.1. Equations of motion

Applying Newton's second law yields the second-order differential equation

$$m_1(\ddot{z} - g) + d_1\dot{z} + k_1 z = F(z,p), \quad z(0) = z_0, \quad \dot{z}(0) = z_1 \tag{2}$$

with the point mass m_1, the spring stiffness k_1 and the constant of gravity g. The viscous damping coefficient d_1 is introduced to reflect damping effects in the system and has to be identified experimentally.

4.2. Pressure dynamics

The state of the air inside the PTA's pressure chamber is determined by its absolute pressure $p(t)$, volume $V(t)$ and temperature $T(t)$. The gas mass inside the pressure chamber is denoted by $m(t)$. Within the range of operating temperature and pressure, it can be assumed that the state obeys the ideal gas law

$$pV = mR_s T \tag{3}$$

where $R_s = 287.058$ J/(kg K) is the specific gas constant of dry air. The material of the textile allows heat flow through its surface such that the change of state behaves between the ideal adiabatic and isothermal conditions, which can be described as a polytropic process (Beater 2007), i.e.

$$pV^{\chi} = const. \tag{4}$$

The polytropic exponent χ lies in the range between 1 (isothermal process) and the isentropic exponent $\kappa = 1.4$ (adiabatic process) and has to be identified experimentally. The total differential of Equation (3) combined with Equation (4) yields the pressure dynamics

$$\dot{p} = \frac{\chi}{V}\left(\dot{m}R_s T - p\dot{V}\right), \quad p(0) = p_0 \tag{5}$$

where T is now assumed to be constant. Since the volume of the pressure chamber depends on the position and pressure, the time derivative of the volume can be expressed as follows:

$$\dot{V} = \frac{\partial}{\partial t}V\left(z(t), p(t)\right) = \frac{\partial V}{\partial z}\dot{z} + \frac{\partial V}{\partial p}\dot{p} = V_z\dot{z} + V_p\dot{p} \tag{6}$$

By substituting Equation (6) in Equation (5), the coupled pressure dynamics become

$$\dot{p} = \frac{\chi(\dot{m}R_s T - \dot{z}pV_z)}{V + \chi pV_p}, \quad p(0) = p_0 \tag{7}$$

4.3. Valve model

A proportional directional control valve regulates the airflow $\dot{m}(t)$. Due to the valve's fast dynamics (the cut-off frequency is greater than 100 Hz), it is assumed that the spool position is directly proportional to the applied voltage which is normalised to $v(t) \in [-1, 1]$, where $v > 0$ means inflation and $v < 0$ deflation of the PTA. Mathematical modelling of the airflow through a valve is based on the assumption of a stationary flow process through an ideal convergent nozzle. Under this assumption, the airflow is governed by three effects. First, the airflow depends on the ratio between the pressure of the upstream air $p_1(t)$ and the downstream air $p_2(t)$ which is described by the flow function $\psi(p_1, p_2)$. An elliptical approximation of the flow function is given by

$$\psi(p_1,p_2) = \begin{cases} \sqrt{1 - \left(\frac{\frac{p_2}{p_1} - b}{1-b}\right)^2}, & \frac{p_2}{p_1} > b \\ 1, & \frac{p_2}{p_1} \le b \end{cases} \tag{8}$$

where b is the critical pressure ratio. Qualitatively, the airflow increases for decreasing pressure ratios until it reaches its maximum at the critical pressure ratio (Figure 4). At this point, the airspeed through the nozzle reaches speed of sound and cannot increase any further. Note that the meaning of upstream and downstream pressure is different for inflation and deflation of the PTA. The second effect governing the airflow through the valve is the variable flow conductance $C(v)$ which depends on the spool position $v(t)$. The flow conductance is

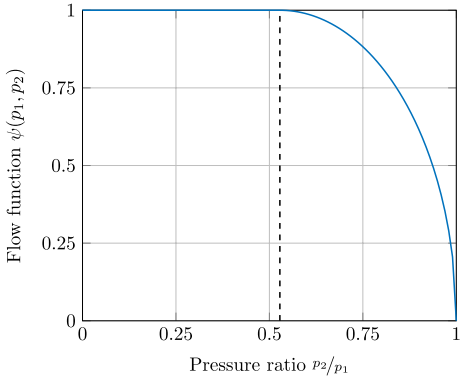

Figure 4. Flow function $\psi(p_1, p_2)$ depending on the pressure ratio between downstream pressure p_2 and upstream pressure p_1.
Note: The dashed line indicates the critical pressure ratio $b = 0.528$ of dry air for an ideal nozzle.

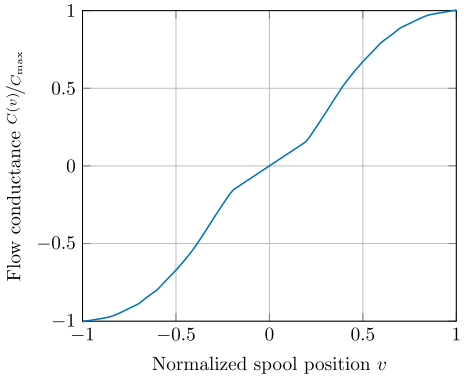

Figure 5. Typical flow conductance $C(v)/C_{max}$ of a valve depending on the spool position, where C_{max} gives the maximum flow through the valve.

governed by the complex geometry of the valve and is usually determined experimentally (Figure 5). Finally, for a fixed spool position and pressure ratio, the airflow is directly proportional to the primary pressure. Combining all effects, the airflow through the valve is given by

$$\dot{m} = \begin{cases} C(v)\psi\left(p_s, p\right)\rho_a p_s, & v > 0 \\ C(v)\psi\left(p, p_a\right)\rho_a p, & v \leq 0 \end{cases} \tag{9}$$

where ρ_a is the density of air at ambient conditions. A more detailed derivation of the valve model can be found in literature, e.g. in (Rao and Bone 2008) or (Maré *et al.* 2000).

4.4. State-space representation

By introducing the state

$$\boldsymbol{x}(t) = \begin{bmatrix} z, & \dot{z}, & p - p_a \end{bmatrix}^T \tag{10}$$

the system dynamics can be expressed compactly in single-input–single-output control affine state-space form

$$\dot{\boldsymbol{x}} = \boldsymbol{f}(\boldsymbol{x}) + \boldsymbol{g}(\boldsymbol{x})u,\ \boldsymbol{x}(0) = \boldsymbol{x}_0 \tag{11a}$$

$$y = x_1 \tag{11b}$$

where $y(t)$ is the controlled variable (output) and $u(t)$ the control effort (input). From Equations (2) and (7) follow the non-linear vector fields

$$\boldsymbol{f}(x) = \begin{bmatrix} x_2 \\ \frac{1}{m_1}\left(F\left(x_1, x_3\right) - k_1 x_1 - d_1 x_2\right) - g \\ -\frac{\chi x_2 (x_3 + p_a) V_{x_1}(x_1, x_3)}{V(x_1, x_3) + \chi(x_3 + p_a) V_{x_3}(x_1, x_3)} \end{bmatrix}, \tag{12a}$$

$$\boldsymbol{g}(x) = \begin{bmatrix} 0 \\ 0 \\ \frac{\chi R_s T}{V(x_1, x_3) + \chi(x_3 + p_a) V_{x_3}(x_1, x_3)} \end{bmatrix}. \tag{12b}$$

The terms $V_{x_i}(x_1, x_3)$ and $F_{x_i}(x_1, x_3)$ denote the partial derivatives of the volume and force maps with respect to the state x_i. The valve model Equation (9) is deliberately not included in the state-space representation. The input $u(t)$ therefore does not reflect the physical input $v(t)$ but the airflow $\dot{m}(t)$ through the valve.

5. Controller design

Motion control of pneumatic systems in general is a challenging task, which is mainly due to the compressibility of air, leading to highly non-linear pressure dynamics. Friction effects as well as the non-linear flow characteristics of the valves impose additional challenges on the control problem. The use of linear controllers usually leads to poor control performance in terms of accuracy, bandwidth and robustness. Therefore, many sophisticated control algorithms have been proposed in literature. For position tracking control of pneumatic cylinders, fuzzy control (Renn 2002), sliding mode control algorithms (Bone and Ning 2007), controllers based on state-dependent Riccati equations (Weickgenannt *et al.* 2010) and control via immersion and invariance (Rapp *et al.* 2012) are found. Wolbrecht and Wells (2014) propose an adaptive control scheme with particular consideration of the valve's dead band. For the control of PAMs, e.g. sliding mode control (Jouppila *et al.* 2014) or flatness-based position-tracking control algorithms (Hildebrandt *et al.* 2002) have been suggested. Beater (2004) presents the mathematical model and control algorithms for pneumatic vane motors. In the present paper, we will employ a combination of flatness-based feedforward control and linear feedback control to solve the control problem.

The control problem can be stated as follows: given the system (11), let the output $y(t)$ asymptotically track the reference trajectory $y_d(t) \in \mathcal{C}^3$ by applying an appropriate

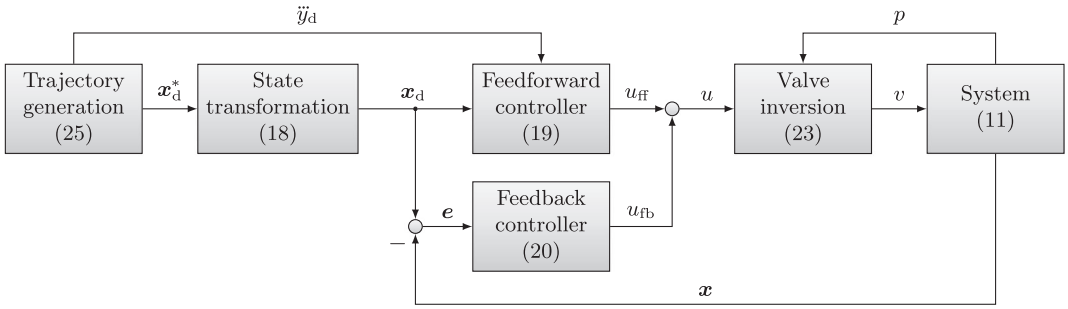

Figure 6. Block diagram of the control concept for PTAs as it is implemented at the test bench.
Note: The numbers in braces reference the corresponding equations.

input $u(t)$ to the system. Generation of suitable reference trajectories is an independent problem that will not be considered here. Instead, it is assumed that $y_d(t)$ and its first three time derivatives are known beforehand. To solve the control problem, a two-degree-of-freedom controller will be used. It consists of a non-linear feedforward controller $u_{ff}(t)$, generating the nominal input required to track the reference trajectory and a linear feedback controller $u_{fb}(t)$ to attenuate disturbances and compensate for modelling errors (Horowitz 1963). The total control effort is the sum of both controllers

$$u = u_{ff} + u_{fb}. \tag{13}$$

Ultimately, the physical input $v(t)$ has to be computed from the control effort $u(t)$. This is done by inversion of the valve model (9) in a subsequent step. In the following subsections, the different components of the controller will be derived step-by-step. For the sake of clarity, the overall structure of the control concept is depicted in Figure 6.

5.1. Flatness-based feedforward control

The basic idea of feedforward controller design for output tracking control is to invert the input/output behaviour of the system. This task is greatly simplified if the system under consideration is differentially flat. A single-input–single-output system is said to be differentially flat, when there exists a (possibly fictitious) flat output as a function of the state, such that the system's state and input can be expressed in terms of the flat output and its time derivatives (Fliess *et al.* 1995). Conveniently, the system (11) is differentially flat with respect to its physical output $y(t)$. The flat coordinates $\boldsymbol{x}^*$(t) are given by the diffeomorphism

$$\boldsymbol{x}^* = \begin{bmatrix} y, & \dot{y}, & \ddot{y} \end{bmatrix}^T = \boldsymbol{\phi}(\boldsymbol{x}), \tag{14}$$

which is obtained by differentiating Equation (11b) with respect to time and using Equation (11a), resulting in

$$\boldsymbol{\phi}(\boldsymbol{x}) = \begin{bmatrix} x_1 \\ x_2 \\ \frac{1}{m_l}\left(F(x_1, x_3) - k_l x_1 - d_l x_2\right) + g \end{bmatrix}. \tag{15}$$

Furthermore,

$$\dddot{y} = \alpha(\boldsymbol{x}) + \beta(\boldsymbol{x})u, \tag{16}$$

with

$$\alpha(\boldsymbol{x}) = \frac{1}{m_l}\begin{bmatrix} F_{x_1}(x_1, x_3) - k_l, & -d_l, & F_{x_3}(x_1, x_3) \end{bmatrix}\boldsymbol{f}(\boldsymbol{x}) \tag{17a}$$

$$\beta(\boldsymbol{x}) = \frac{1}{m_l}\begin{bmatrix} F_{x_1}(x_1, x_3) - k_l, & -d_l, & F_{x_3}(x_1, x_3) \end{bmatrix}\boldsymbol{g}(\boldsymbol{x}) \tag{17b}$$

Given the desired output trajectory $y_d(t)$ and its time derivatives, the desired state trajectory $x_d(t)$ is computed by the inverse transformation

$$\boldsymbol{x}_d = \boldsymbol{\phi}^{-1}(\boldsymbol{x}_d^*) \tag{18}$$

To compute $\phi^{-1}(\cdot)$ from Equation (15) the force map $F(x_1, x_3)$ has to be solved for x_3. In case of the polynomial approximation Equation (1a), this can be done explicitly. For higher order polynomials or other types of approximations, numerical solution might be necessary.

Finally, by solving Equation (16) for $u(t)$ and applying the desired trajectories $\boldsymbol{x}_d(t)$ and $\dddot{y}_d(t)$, the feedforward control law reads

$$u_{ff} = \frac{\dddot{y}_d - \alpha(\boldsymbol{x}_d)}{\beta(\boldsymbol{x}_d)}. \tag{19}$$

5.2. Linear feedback control

To attenuate disturbances and compensate for modelling errors, the controller is augmented by a linear feedback controller. The feedback controller has a cascading structure, consisting of an inner pressure controller and an outer position controller. The proportional pressure controller stabilises the pressure along a given reference trajectory. The integral position controller corrects this reference trajectory, based on the position error, i.e. the reference pressure is increased when the position is below the desired position and vice versa. Hence, the feedback controller is given by

$$u_{fb} = k_P\left(x_{3,d} - x_3 + k_I \int_0^t \left(x_{1,d} - x_1\right) \mathrm{d}\tau\right). \tag{20}$$

The reference trajectories $x_{1,d}(t)$ and $x_{3,d}(t)$ are obtained from (18), such that consistency between feedforward and feedback control is guaranteed. The controller gains were adjusted heuristically. First, the proportional gain k_P is increased for $k_I = 0$, until audible valve chattering occurs and then reduced by about 20%. Then, the integral gain k_I is increased from zero until the steady-state error vanishes in reasonable time.

5.3. Valve inversion

In the system model given by Equation (11), the control effort $u(t)$ corresponds to the airflow $\dot{m}(t)$, albeit the physical input to the system is the normalised spool position $v(t) \in [-1, 1]$ of the valve. While it is always possible to compute the airflow $\dot{m}(t)$ from the spool position $v(t)$ according to Equation (9), the opposite does not apply. From physical considerations it is obvious that there exist certain limits on the airflow. First, the maximum airflow through the valve is bounded by the variable flow conductance $C(v)$, which gives a maximum possible airflow for every spool position (Figure 5). Second, the airflow depends on the ratio between upstream and downstream pressure, which is described by the flow function Equation (8). For example, when the downstream and upstream pressure are equal, the airflow $\dot{m}(t) = 0$ for all spool positions $v(t)$. Third, the airflow is proportional to the absolute value of the primary pressure, i.e. increasing the primary pressure increases the airflow for a fixed pressure ratio and valve position. Hence, the control effort is limited by the dynamic input constraints

$$u_{\min}(\boldsymbol{x}) \leq u \leq u_{\max}(\boldsymbol{x}), \tag{21}$$

where

$$u_{\max}(\boldsymbol{x}) = C(1)\psi\left(p_s, x_3\right)\rho_a p_s \tag{22a}$$

$$u_{\min}(\boldsymbol{x}) = C(-1)\psi\left(x_3, p_a\right)\rho_a x_3 \tag{22b}$$

If Equation (21) holds, the valve model can be inverted by

$$v = \begin{cases} C^{-1}\left(\frac{u}{\psi(p_s, x_3)\rho_a p_s}\right), & u > 0 \\ C^{-1}\left(\frac{u}{\psi(x_3, p_a)\rho_a x_3}\right), & u \leq 0 \end{cases} \tag{23}$$

where $C^{-1}(\cdot)$ is the inverse map of the flow conductance. If Equation (21) is violated, the spool position is set to $v = \pm 1$ for $u > 0$ and $u < 0$, respectively, in order to obtain the maximum possible airflow. Note, that while the lower limit $u_{\min}$ is determined by the valve's characteristics, the upper limit $u_{\max}$ may be easily increased by increasing the supply pressure p_s (cf. Equation (22)). For a given reference trajectory, violation of Equation (21) can be checked beforehand by evaluating Equation (19). If Equation (21) is violated, the given reference trajectory is not exactly realisable. From a practical point of view, $u_{ff}(t)$ should not exceed about 80% of the available control effort in order to leave some reserve for the feedback controller. The effect of input constraint violation will be demonstrated in the experimental validation.

6. Experimental validation

For experimental validation of the suggested motion control algorithm for PTAs, point-to-point motions are considered. These are motions from position $y(t_0) = y_0$ to $y(t_1) = y_1$ with $t_1 > t_0$, where the system is at rest before and after each motion cycle, meaning that

$$y^{(i)}(t_0) = y^{(i)}(t_1) = 0, \quad i = 1 \ldots n. \tag{24}$$

This type of motion was chosen because it reflects a common task in industrial applications. From Equation (19) it follows that the reference trajectory $y_d(t)$ has to be three times continuously differentiable, in order to be exactly realisable. These requirements are met by polynomial reference trajectories of the form

$$y_d(t) = y_0 + (y_1 - y_0)\sum_{i=4}^{7} p_k\left(\frac{t}{T}\right)^i, \quad t \in (t_0, t_1), \tag{25}$$

where $T = t_1 - t_0$ is the transition time, and p_k are the polynomial coefficients. Since the reference trajectories are planned before each motion cycle, the time derivatives of Equation (25) can be obtained analytically.

The experimental results show four different motion cycles with the transition times $T_1 = T_2 = 2$ s and $T_3 = T_4 = 0.5$ s, respectively (Figure 7). In the figure, the duration of each motion cycle is marked with a light grey background. During the first motion cycle, the position is increased, meaning that the PTA has to be inflated. The results show, that the position trajectory $y(t)$ closely follows its reference trajectory with the maximum error smaller than 0.2 mm during this motion cycle. The pressure trajectory $p_{rel}(t)$ also follows its reference trajectory but shows a small offset. This offset is caused by the output of the integral position controller, which is added to the pressure reference trajectory, indicating that the actual pressure required to achieve the desired position is smaller than the pressure predicted by the model. A possible explanation is that the stiffness of the springs is smaller than the nominal stiffness used in the model or that the force map underestimates the force of the PTA. The control input $u(t)$, which corresponds to the desired mass flow to the pressure chamber, is the sum of the outputs of the feedforward and feedback controllers. In the first motion cycle, the control signal is dominated by the feedforward controller and the feedback controller only makes minor corrections. In the second motion

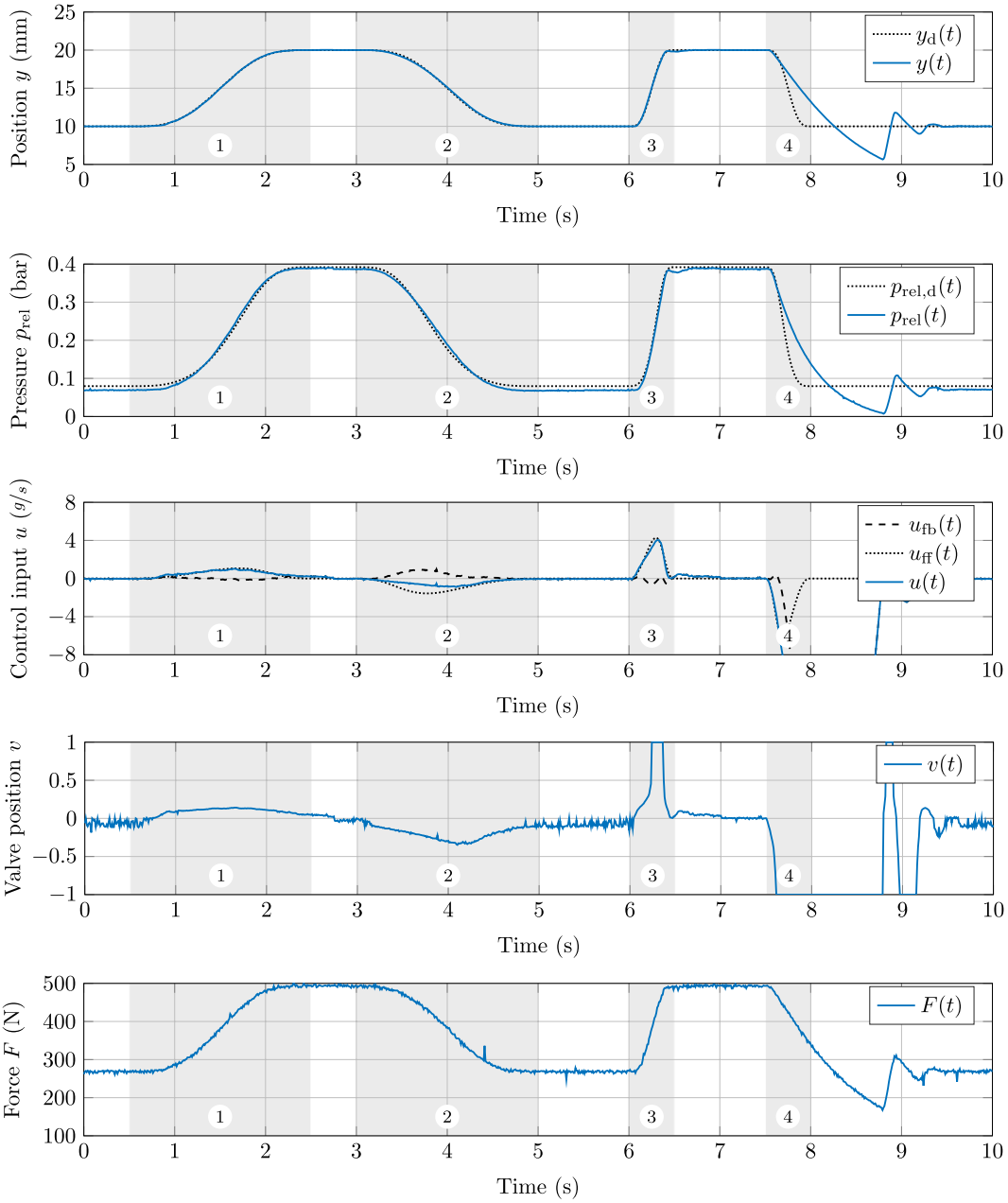

Figure 7. Experimental results of four motion cycles with polynomial reference trajectories of transition times $T_1 = T_2 = 2$ s and $T_3 = T_4 = 0.5$ s (light grey background indicates duration of motion cycles).

cycle, the position is decreased, meaning that the PTA has to be deflated. Again, the position and pressure trajectories closely follow their reference trajectories. The control input, however, is no longer dominated by the feedforward controller but significantly corrected by the feedback, indicating that the model overestimates the required mass flow to decrease the pressure. In the third and fourth motion cycles, the transition time is reduced significantly, such that the dynamic input constraints are violated. The control signal $u(t)$ is exceeding its limits, leading to a saturation of the valve signal $v(t)$. In the third motion cycle the reference trajectories can still be followed. In the forth motion cycle, however, the saturation effect is more pronounced, yielding substantial deviation from the reference trajectories. This can be explained by the fact that the maximum possible mass flow depends on the primary pressure, which is lower for deflation ($p_1 = p$) than for inflation ($p_1 = p_s$). In the proposed control scheme, the input saturation leads to integrator wind-up, such that the pressure and position trajectories shoot over their references until the integrator is cleared. This undesirable behaviour could be improved by the use of well-known anti-wind-up strategies.

7. Conclusion

The present paper introduces the novel PTA developed by the Institute of Textile Technology and Process Engineering Denkendorf. A mathematical model describing the static and dynamic behaviour of an exemplary motion system employing a rectangular 200 × 200 mm PTA has been derived. Precise

knowledge of the PTA's nonlinear force and volume maps is vital to achieve high model accuracy. In the present paper, these maps have been determined experimentally. Future work on PTAs includes the computational derivation of the nonlinear maps for arbitrary geometries of the pressure chamber to avoid time-consuming experiments. Based on the model, a two-degree-of-freedom motion controller has been derived. Experimental results indicate, that the suggested controller allows precise control of the PTAs motion, as long as the dynamic input constraints, imposed by the maximum mass flow through the valve, are not violated. Since the input constraints are more pronounced for deflation of the PTA, future work includes the use of vacuum nozzles to extend the input constraints. Furthermore, the effects of input saturation can possibly be alleviated by the use of anti-wind-up strategies.

Disclosure statement

No potential conflict of interest was reported by the authors.

Funding

This work was funded by the German Research Foundation (Deutsche Forschungsgemeinschaft) under grant SA-847/8-2 and PL 120/21-2 as part of the research group FOR-981.

Notes on contributors

Michael Heidingsfeld received the Dipl.-Ing. degree in mechanical engineering from the Karlsruhe Institute of Technology, Germany, in 2012. He is currently a research assistant at the Institute for System Dynamics, University of Stuttgart, Germany, where he is also working towards the PhD degree. His research interests include modelling, identification and control of mechatronic systems, particularly in the field of adaptive structures.

Ryosuke Horio received the B.Eng. degree from Toyohashi University of Technology, Japan, in 2014. In 2015, he participated in a double-degree programme with the University of Stuttgart, Germany, where he spent two semesters at the Institute for System Dynamics. He is currently with the Systems Engineering Laboratory at Toyohashi University of Technology. His research interests include optimal control and robotics, particularly control of legged robots.

Bastian Baesch received his Dipl.-Ing. degree in mechanical engineering from the University of Stuttgart, Germany, in 2009. He is currently a team leader at the Institute of Textile Technology and Process Engineering Denkendorf, Germany where he is also working towards the PhD degree. His research interests include sensory and actuatory textiles as well as light engineering aspects of textiles.

Christoph Riethmüller received his Dipl.-Ing. degree in mechanical engineering from the University of Stuttgart, Germany, in 1998. He is currently a management assistant and the head of the Business Units Technology Integration (*inter alia* PTAs), Winding Technology and Denkendorf Future Workshop. His research interests include cross-technology product developments, pneumatic textiles in general and light engineering aspects of textiles.

Götz T. Gresserc received the Dipl.-Ing. degree in mechanical engineering from the University of Stuttgart, Germany, in 1991 and the Ph.D. degree in 1998. Since 2013 he is a full professor at the University of Stuttgart and the head of the Institute of Textile Technology and Process Engineering Denkendorf, Germany, a member of the Managing Board of The German Institutes of Textile and Fiber Research Denkendorf (DITF), Germany, as well as the head of ITV Denkendorf Product Service Ltd., Germany. His research interests include basic and practice-oriented research related to all stages of the textile production chain, from raw material to final products.

Oliver Sawodny received the Dipl.-Ing. degree in electrical engineering from the University of Karlsruhe, Germany, in 1991 and the PhD degree from the University of Ulm, Germany, in 1996. In 2002, he became a full professor at the Technical University of Ilmenau, Germany. Since 2005, he has been the director of the Institute for System Dynamics, University of Stuttgart, Germany. His current research interests include methods of differential geometry, trajectory generation and applications to mechatronic systems.

References

Beater, P., 2004. Modelling and control of pneumatic vane motors. *International Journal of Fluid Power*, 5 (1), 7–16.

Beater, P., 2007. *Pneumatic drives: system design, modeling and control*. Berlin: Springer.

Bone, G.M. and Ning, S., 2007. Experimental comparison of position tracking control algorithms for pneumatic cylinder actuators. *IEEE/ASME Transactions on Mechatronics*, 12, 557–561.

Daerden, F. and Lefeber, D., 2001. The concept and design of pleated pneumatic artificial muscles. *International Journal of Fluid Power*, 2 (3), 41–50.

Fliess, M., *et al.*, 1995. Flatness and defect of non-linear systems: introductory theory and examples. *International Journal of Control*, 61 (6), 1327–1361.

Hildebrandt, A., *et al.*, 2002. A flatness based design for tracking control of pneumatic muscle actuators. *In: 7th International Conference on Control, Automation, Robotics and Vision*. Singapore, 1156–1161.

Horowitz, I.M., 1963. *Synthesis of feedback systems*. New York, NY: Academic Press.

Jouppila, V.T., *et al.*, 2014. Sliding mode control of a pneumatic muscle actuator system with a PWM strategy. *International Journal of Fluid Power*, 15 (1), 19–31.

Maré, J.-C., Geider, O. and Colin, S., 2000. An improved dynamic model of pneumatic actuators. *International Journal of Fluid Power*, 1 (2), 39–49.

Rao, Z. and Bone, G.M., 2008. Nonlinear modeling and control of servo pneumatic actuators. *IEEE Transactions on Control Systems Technology*, 16, 562–569.

Rapp, R., *et al*., 2012. Nonlinear adaptive and tracking control of a pneumatic actuator via immersion and invariance. In: *51st IEEE Conference on Decision and Control*. Maui, 4145–4151.

Renn, J.-C., 2002. Position control of a pneumatic servo cylinder using fuzzy-sliding surface controller. *International Journal of Fluid Power*, 3 (3), 19–26.

Weickgenannt, M., *et al*., 2010. Application of SDRE control to servopneumatic drives. *In*: *IEEE International Conference on Control Applications*. Yokohama, 1725–1730.

Wolbrecht, E. and Wells, L., 2014. Adaptive pneumatic control with spool deadband compensation. *International Journal of Fluid Power*, 13 (3), 25–37.